A new approach for target classification of Ka-band radar data

Gerd Teschke[1], **Ulrich Görsdorf**[2], **Philipp Körner**[3], **and Dennis Trede**[3]

[1]Konrad-Zuse-Zentrum für Informationstechnik Berlin (ZIB), Research Group Inverse Problems in Science and Technology, Berlin (Germany).
[2]Deutscher Wetterdienst (DWD), Meteorologisches Observatorium Lindenberg (Germany)
[3]Universität Bremen, Zentrum für Technomathematik, Bremen (Germany)

1 Introduction

Millimeter-radars have been established as valuable systems for remote sensing of cloud structure and processes during the last two decades (Kropfli and Kelly, 1996). They measure profiles of intensity of particle backscattered signals and their Doppler shift, which can be used to derive information about the particle size and concentration as well as about their motion. Some radars have the capability for polarimetric measurements which provides additional information about the particle shape and/or their orientation.

The derivation of macro- and microphysical cloud parameters is restricted by the fact, that millimeter-radars are not only sensitive for cloud or rain droplets but for all particles in the atmosphere as for insects, dust or pollen (named also as "atmospheric plankton"). Furthermore, the reflectivity is proportional to the 6th power of particle diameter. That means that few relatively large particles in the radar volume can dominate the radar signal. Therefore, the detection of cloud base heights on the base of radar reflectivities is impossible:

- in situations of precipitation,
- clouds with falling drizzle,
- if insects (or other non-hydrometeors) are present.

These problems can be overcome by combination of radar measurements with them of optical systems as ceilometer, which is currently the standard technique for unambiguous cloud base detection (Uttal et al., 1995; Clothiaux et al., 1995, 2000; Hogan et al., 2001; Sievers et al., 2002; Uttal et al., 2005).

Another way for insect filtering, independently on any other system, is the use of additional radar parameters as for example the linear depolarization ratio (LDR), which is considerable higher for insects than for clouds (Khandwalla et al., 2003) or Doppler spectra which can have typical signatures for different targets or their compositions.

Also the derivation of microphysical parameters (e.g., liquid water content) only on the base of reflectivity values is imprecise, when there is no separation between cloud and rain droplet regimes (Krasnov and Russchenberg, 2003; Russchenberg and Boers, 2003).

The goal of this paper is to propose a sophisticated classification algorithm that uses spectral information of a cloud radar system only and performs

- a decomposition into atmospheric and clutter signals, and
- a classification of hydrometeors of different droplet regimes.

The capabilities of the suggested algorithm are verified by processing measurements taken at the Meteorological Observatory Lindenberg which is operating a 35.5 GHz coherent receiving and polarimetric cloud radar (MIRA36) to measure vertical profiles of reflectivity, Doppler velocity, spectral width and linear depolarisation ratio (LDR) between 250 m and 12 km with a temporal resolution of 10 s. The system is in continuous operation and saves regularly the moments and the LDR, and in addition the Doppler spectra for two hours per week.

2 System characteristics

MIRA36 is based on a magnetron transmitter providing a peak power of 30 kW and an excellent pulse shape. It has two symmetrical receivers for simultaneously receiving of co- and cross-polarized signals, a vertically pointed cassegrain antenna with a polarization filter and a computer including a

Correspondence to: Gerd Teschke
(teschke@zib.de)

DSP board for data acquisition and processing. For diagnostic and control purposes the most important system parameters are measured and saved by the radar PC. All components are installed in a trailer. For calibration purposes the transmitted power is measured continuously. The receiver calibration is derived from the receiver noise measured at 15 km height (where normally no meteorological signal is detected) and the noise figure is determined from time to time by an external calibrated noise source. More details are given in Table 1.

	MIRA36
Frequency	35.5 GHz
Peak Power	30 kW
Noise figure	6.3 dB
+ loss in receiver path	+3 dB image noise
Loss in transmit path	1.3 dB
Antenna type	Cassegrain with polarization filter
Antenna diameter	1 m
Antenna gain	49 dB
Beam width	0.55
Pulse length	100, **200** and 400 ns
Vertical resolution	15, **30** and 60 m
Pulse repetition frequency	2.5, **5**, 7.5, 10 kHz
FFT-Length	128, **256**, 512 and 1024
Min. measuring height	150 m (**240 m**)
Max. measuring height	15 km (**12 km**)
Averaging time	0.05 - 60 sec (**10 sec**)
Sensitivity at 5 km (0.1 sec)	-40.3 dBZ

Table 1. Technical characteristics of the MIRA36 (highlighted are standard settings)

3 Mathematical Concepts

The basis for identifying clutter components (insects etc.) is the analysis of the Fourier power spectrum for both the copolarized and crosspolarized signal, s_{HH} and s_{VH}, and its moments

$$L_{HH} = \int s_{HH}(\omega)d\omega, \;\; L_{VH} = \int s_{VH}(\omega)d\omega,$$

$$E = \int \omega s_{HH}(\omega)d\omega, \;\; V = \int (\omega - E)^2 s_{HH}(\omega)d\omega \;,$$

and finally the classical linear depolarization ratio

$$\mathrm{LDR} = 10\log\left(\frac{L_{VH}}{L_{HH}}\right).$$

As a novelty, we introduce a new quantity - the *localized* linear depolarization ratio. This new ratio requires the use of spectral energy quants of width 2δ,

$$L^{\delta}_{HH}(x) = \int_{x-\delta}^{x+\delta} s_{HH}(\omega)d\omega,$$

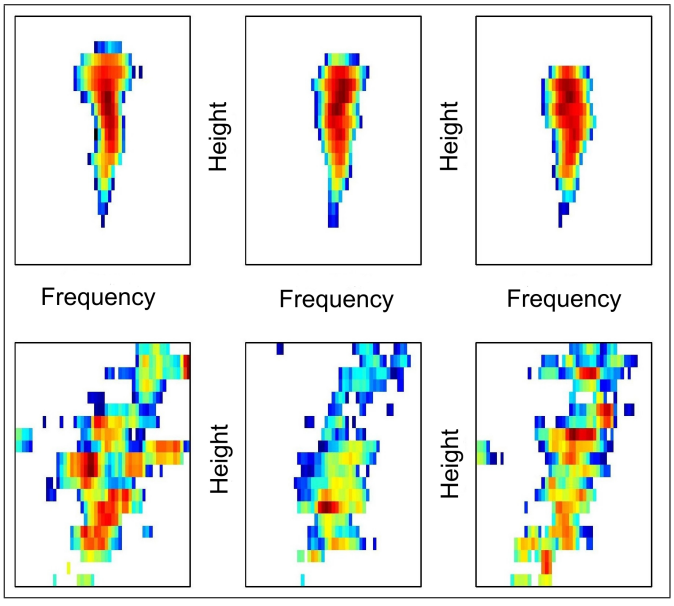

Fig. 1. Spatial-temporal consistency of Fourier power spectra. Top row: Fourier power spectra of hydrometeor returns for three subsequent time steps, bottom row: Fourier power spectra of atmospheric plankton for three subsequent time steps.

$$L^{\delta}_{VH}(x) = \int_{x-\delta}^{x+\delta} s_{VH}(\omega)d\omega,$$

and is then defined by

$$\delta - \mathrm{LDR}(x) = 10\log\left(\frac{L^{\delta}_{VH}(x)}{L^{\delta}_{HH}(x)}\right).$$

These ratios allow a localized spectral analysis in order to separate signal components from different target types. This is especially useful in cases where one individual spectrum contains returns caused by both plankton clutter and hydrometeors.

In order to identify different targets, we propose to proceed in two steps:

1. Decomposition into atmospheric and clutter signals

We apply a preprocessing step that uses a spatial-temporal consistency test in which we use the fact that the spectra of plankton fluctuates with respect to time and space much stronger than the spectra of hydrometeors, see Figure 1. This test yields for each spectral point a specific hydrometeor-confidence value. The second parameter is the localized δ-LDR. On the basis of these two parameters a simple classification rule induces a removal of plankton components. In contrast to the use of a simple LDR thresholding, the application of δ-LDR avoids the removal of hydrometeor information at heights where plankton was detected, see example in Figure 2.

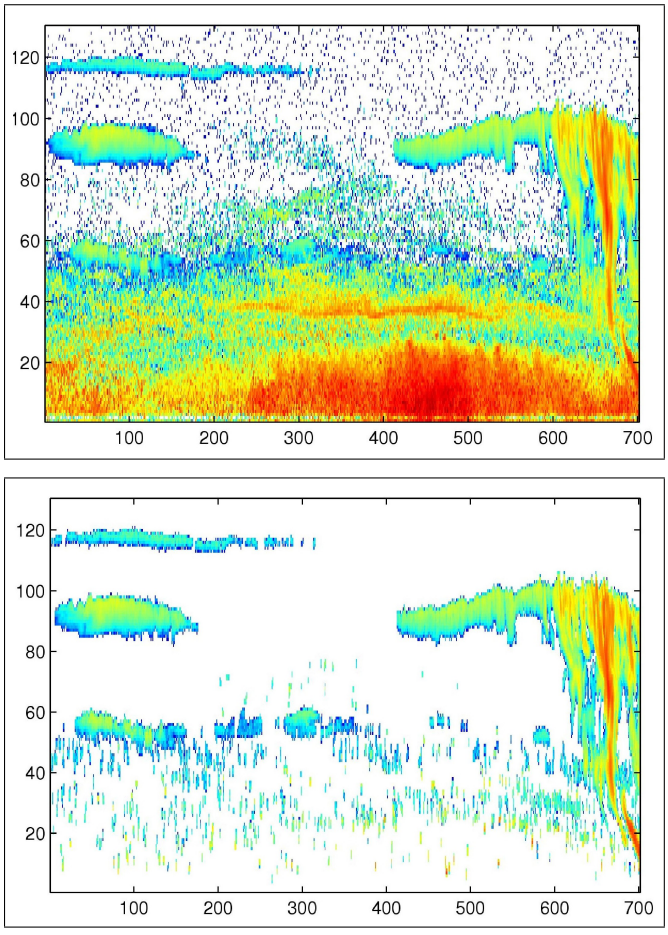

Fig. 2. Application of the decomposition procedure. Top: time-height cross section of original reflectivities, bottom: after plankton removal (axis convention: x-axis $\sim$ seconds, y-axis $\sim$ range gates, 1 range gate = 30m).

2. Classification of hydrometeors

The final step is the classification of the hydrometeor regime. As long as the signal contains just returns from hydrometeors of one individual species, the spectrum looks quite unimodal. However, in many situations, returns from several species produce sort of multi-modal spectrum (a composition of several Gaussian functions). In this case, the peaks have to be separated. The separation process is essentially related to a nonlinear Gauss fit of the (noisy) Fourier power spectra. Typically, the problems reads as

$$\|s(\omega) - \sum_j x_j \exp(-(\omega - \mu_j)^2/(2\sigma_j^2))\|^2 \to \min \ ,$$

where the minimization has to be done with respect to x_j, μ_j and σ_j. This is, however, a very numerically intensive task which often fails when choosing a wrong initial guess. Moreover, since the spectra are noisy, this optimization functional forces also the fit of side lobes of essential main Gaussian peaks, which is not meaningful and ends up in much higher number of Gaussians than really being within the spectra. To this end, we suggest a functional that avoids all these drawbacks (nonlinearity, non-essential Gaussians, side lobe problems). First, we provide a relatively rich dictionary A of preselected Gaussian atoms for which an optimal fit can be achieved when minimizing

$$\|s - Ac\|^2$$

with respect to c (where c stands for a vector of coefficients). Next, we add a constraint $\|\cdot\|_1$ that promotes sparsity of c (in order to avoid non-essential Gaussians), and, moreover, a constraint that penalizes a side lobe fitting. All this results in the following optimization problem

$$\|s - Ac\|^2 + \alpha\|c\|_1 + \beta\|Bc\|^2 \to \min \ .$$

By means of the method of Gaussian surrogate functionals, a minimization of this cost functional amounts to Landweber iteration which soft shrinkage applied in each step,

$$c_{n+1} = S_\alpha(c_n + (A + \beta B)^T(s - (A + \beta B)c_n)),$$

with

$$S_\alpha(x) = \begin{cases} x - \alpha \ , & x \geq \alpha \\ x + \alpha \ , & x \leq -\alpha \end{cases}.$$

Convergence in norm of this scheme is shown in Daubechies and Teschke (2005) using results shown in Daubechies et al. (2004). On the basis of the resulting limit c^* we obtain a representation of each individual spectrum s by Ac^*. The Gaussian atoms being selected to represent s determine now the different droplet regimes at particular heights and times.

4 Numerical Evaluation

In order to show the applicability of the proposed two-step algorithm, we consider two particular data sets. The first example (see Figure 2) was measured at the Meteorological Observatory Lindenberg on 07/27/2005 and shows the presence of atmospheric plankton. The application of the decomposition step successfully removes almost all clutter components, whereas cloud and rain echoes remain. The second example (see Figure 3) was measured on 04/05/2005 and shows the presence of all: clouds, drizzle, and plankton. The application of the decomposition and hydrometeor classification yields convincing results.

5 Conclusions

In this paper, we have presented a new algorithm for Ka-band radar target classification which does not require any additional measurement devices. The algorithm shows encouraging results for the identification of atmospheric plankton and the classification of different droplet regimes.

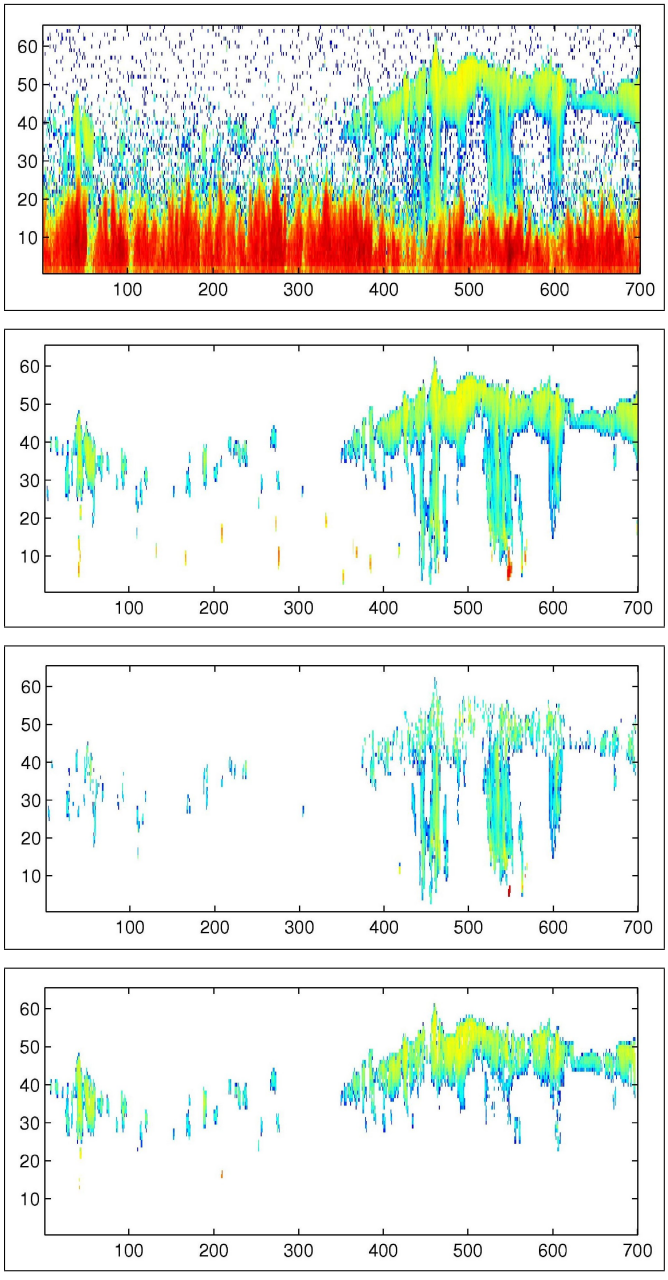

Fig. 3. Application of the full algorithm. From top to bottom: time-height cross sections of original reflectivities, after plankton removal, reflectivities characterizing rain or drizzle, reflectivities characterizing clouds (axis convention: x-axis $\sim$ seconds, y-axis $\sim$ range gates, 1 range gate = 30m).

The essential innovations are two mathematical concepts: at first, the δ-LDR, and secondly, a refined fitting tool for multi modal spectral analysis.

The proposed algorithm was verified on several data sets (extensive test computations/evaluations are planned) and we judge the capabilities of this new procedure as very promising.

Acknowledgements. This first author was supported by DFG 354/1-2 and DFG 354/3-1.

References

Clothiaux, E., Miller, M., Albrecht, B., Ackerman, T., Verlinde, J., Babb, D., Peters, R., and Syrett, W.: An evaluation of a 94-GHz radar for remote sensing of cloud properties, J. Atmos. Oceanic Technol., 12, 201–229, 1995.

Clothiaux, E. E., Ackerman, T. P., Mace, G. G., Moran, K. P., Marchand, R. T., Miller, M. A., and Martner, B. E.: Objective determination of cloud heights and radar refectivities using a combination of active remote sensors at the ARM CART sites, J. Appl. Meteor., 39, 645–665, 2000.

Daubechies, I. and Teschke, G.: Variational image restoration by means of wavelets: simultaneous decomposition, deblurring and denoising, Applied and Computational Harmonic Analysis, pp. 1–16, 2005.

Daubechies, I., Defrise, M., and DeMol, C.: An iterative thresholding algorithm for linear inverse problems with a sparsity constraint, Comm. Pure Appl. Math, 57, 1413–1541, 2004.

Hogan, R. J., Jakob, C., and Illingworth, A. J.: Comparison of ECMWF winter-season cloud fraction with radar derived values, J. Appl. Meteor., 40, 513–525, 2001.

Khandwalla, A., Sekelsky, S., and Quante, M., eds.: Algorithms for filtering insect echoes from cloud radar measurements, Thirteenth ARM Science Team Meeting Proceedings, Broomfield, Colorado, 2003.

Krasnov, O. and Russchenberg, H., eds.: Retrieval of the LWC in water clouds with radar and lidar, ISTP, Sixth International Symposium on Tropospheric Profiling; Needs and Technologies, Leipzig, 2003.

Kropfli, R. and Kelly, R.: Meteorological research application of MM-wave radar, Meteorol. Atmos. Phys., 59, 105–121, 1996.

Russchenberg, H. and Boers, R.: Radar sensor synergy for cloud studies; Case study of water clouds, chap. 8, pp. 235–254, Weather Radar, Springer, 2003.

Sievers, O., Meywerk, J., and Quante, M., eds.: Statistics of non-precipitating daytime clouds, based on 95 GHz cloud radar measurements during the BBC campaign, Proceedings of ERAD, ERAD 2002, 2002.

Uttal, T., Clothiaux, E. E., Ackerman, T. P., Intrieri, J. M., and Eberhard, W. L.: Cloud boundary statistics during FIRE II, J. Atmos. Sci., 52, 4276–4284, 1995.

Uttal, T., Frisch, S., Wang, X., Key, J., Schweiger, A., Sun-Mack, S., and Minnis, P.: Comparison of Monthly Mean Cloud Fraction and Cloud Optical depth Determined from Surface Cloud Radar, TOVS, AVHRR, AND MODIS over Barrow, Alaska, in: AMS 8th Conference on Polar Meteorology, San Diego, CA, edited by Uttal, T., Environmental Technology Laboratory, Boulder, CO, 2005.